HT2024-131037

EXPLORATION OF THE EFFECTS OF NANOSCALE SURFACE MORPHOLOGY VARIATIONS ON ONSET OF BUBBLE NUCLEATION IN WATER DROPLETS IMPINGING AND BOILING ON NANOSTRUCTURED SURFACES

Anisa D. Silva and Van P. Carey

Mechanical Engineering Department University of California, Berkeley, CA

ABSTRACT

Nanostructured hydrophilic surfaces can enhance boiling processes due to the liquid wicking effect of the small surface structures, but consistently uniform nanoscale interstitial spaces would provide very few heterogeneous nucleation sites, which would require high superheat to activate in, for example, liquid water. Experiments indicate that surfaces of this type initiate onset of nucleate boiling at relatively low superheat levels, implying that larger-than-average interstitial spaces exist, apparently as a consequence of larger micron-scale variations of the surface structure or surface chemistry (wetting) resulting from the fabrication process. The investigation summarized here explores the potential correlation between nanostructured surface morphology variations and onset of nucleation. A zinc oxide nanostructured coating was fabricated on a copper substrate for experiments and analysis in this study. The coated surface was subjected to water droplet deposition tests to evaluate wicking and contact angle, followed by vaporization tests at varying surface superheat levels, and extensive electron microscopy imaging of the surface. The results of the vaporization experiments determined the variation of mean heat flux to the droplet as a function of superheat, and high-speed videos documented the superheat at which onset of nucleate boiling (ONB) occurs and variation of nucleation site density with superheat. Image analysis of the electron microscopy images were used to assess the variability of pore size and surface complexity (entropy) over the surface. By determining macroscope bubble nucleation and boiling performance from measured data and high-speed video records for these surfaces, and simultaneously analyzing the morphology of that surface at the micro/nano scale, our data demonstrates the correlation between surface morphology variations and ONB and nucleate boiling active site density. Specifically, our results indicate that increased irregularities in the surface morphology correspond to enhanced probability of nucleation onset and an increase in active nucleation site density as superheat increases. Our data indicates the range of irregularity number density values (number per square millimeter) and the imperfection features that give rise to consistent low superheat ONB ($\sim 15^{\circ}C$), leads to a robust increase in active site density during nucleate boiling as super heat increases. This information can help guide development of enhanced boiling surfaces by providing insight into the frequency of nanosurface morphology variations, per square millimeter, that enhance nucleation onset while also providing enhanced wicking and low contact angle over most of the surface. The implication of these results for design of different types of enhanced boiling surfaces is also discussed.

NOMENCLATURE

Roman letters

Thermal conductivity of liquid water[W m⁻¹ K⁻¹] k_{l}

Number of nucleation sites, dimensionless n

 n'_{a} Observed nucleation site density [mm⁻²]

Prandtl number of the liquid, dimensionless

Heat flux [W cm⁻²]

 $Pr_l \\ q^{"} \\ ar{q}^{"} \\ ar{r}^{*}$ Mean heat flux [W cm⁻²]

Critical radius [mm]

Heated wall temperature [°C]

Saturation temperature [°C]

 $\Delta T_{sat} = T_w - T_{sat}$ Surface superheat [°C]

initial droplet volume $[\mu L]$ V_{d0}

Greek letters

constant $[m^{-2} \circ C^{-1}]$

constant, dimensionless

1. INTRODUCTION

As a basis for analysis of morphology and corresponding bubble nucleation behavior, fabrication of the ZnO nanostructured surfaces and droplet evaporation experiments were completed. The fabrication and experiments of the substrates closely follows similar previous researched recent researchers' works which have been developed, refined, and adapted to other applications [1–5]. The most recent use of the process, [6], most closely resembles fabrication and experiments performed in this

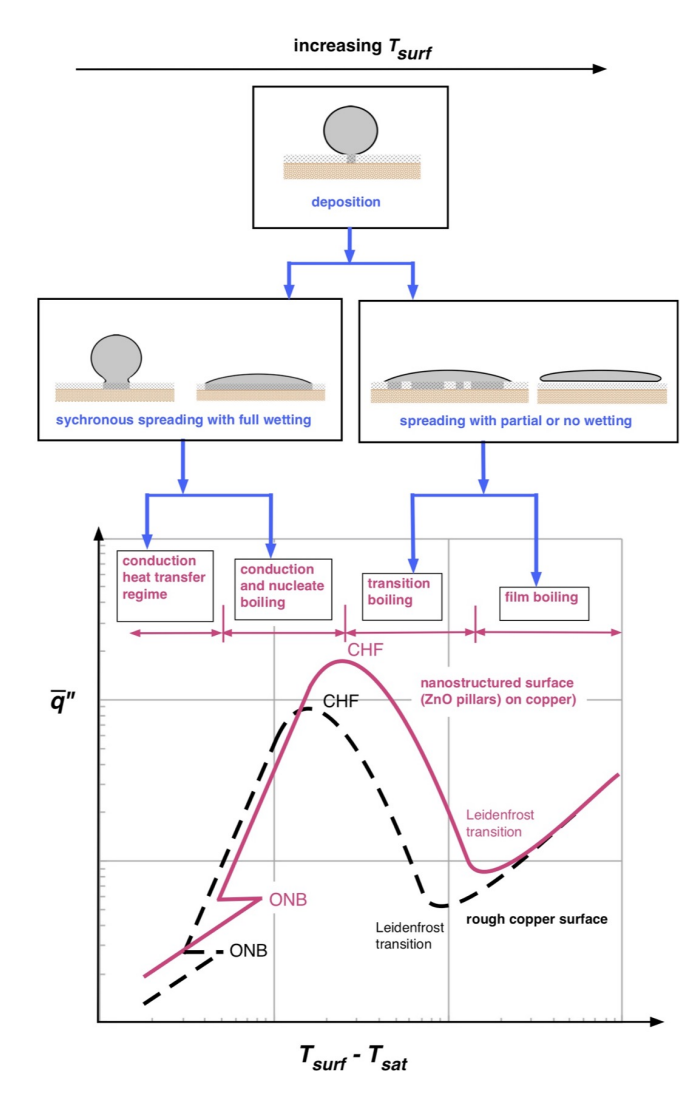


FIGURE 1: Process sequence for droplet evaporation on nanostructured surfaces (nanostructured surface boiling curve based on quenching experiment pool boiling data from Carey, et al. [1])

study. Extensive steps of the procedure can be found in the referenced works and any deviations performed in this research will be commented on.

The work summarized here focuses on the vaporization/boiling process associated with liquid water droplets deposition on a superheated surface. In an earlier investigation, Carey, et al. [1] analyzed features and mechanisms of droplet vaporization on superheated nanostructured surfaces, and compared them to pool boiling under similar conditions. Their comparison of the droplet vaporization mean heat flux and pool boiling data for quenching experiments for the same surface under comparable conditions indicated a close correspondence between the boiling features in these two cases, as depicted in Fig. 1.

Observations and data from this earlier study indicate that the boiling features of vaporization of deposited water droplets on superheated surfaces are strongly similar to those for pool boiling observed in quenching experiments under similar conditions. Droplet deposition experiments therefore can be used to explore nucleate boiling mechanisms near the onset of nucleate boiling

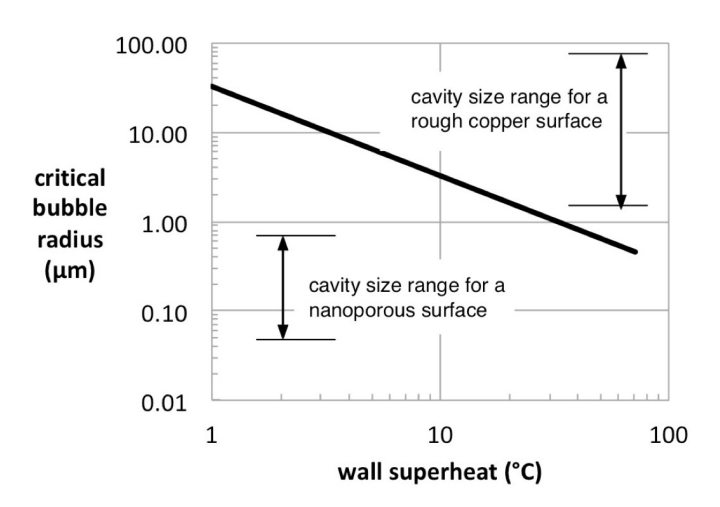


FIGURE 2: Model prediction of critical bubble radius with wall superheat for water at atmospheric pressure, based on Eq. 1

while providing imaging access close to the surface, which allows more effective use of optical methods to obtain image information about the process. In addition, these investigators noted that, for the nanostructured coating they considered, observed the onset of nucleate boiling (ONB) typically in the $10\text{-}15\,^{\circ}\text{C}$ range. Conventional ONB theory is generally based on the premise that the necessary condition for active heterogeneous nucleation sites is that cavities exist on the surface that have an effective mouth radius (and therefore a bubble interface radius) greater than the critical radius for the wall superheat [7]. The variation of critical radius $r_{i,crit}$ with superheat can be predicted by a simple thermodynamics-based model [7]

$$r_{i,crit} = \frac{2\sigma T_{sat}}{\rho_l h_{lv} (T_{surf} - T_{sat})} \tag{1}$$

Where T_{surf} is equivalent to T_w in this study. The predicted variation of $r_{i,crit}$ with wall superheat for water at atmospheric pressure is shown in Fig. 2.

Of particular note here is that superheat of about 10°C corresponds to a critical radius of about 5 μm . Cavities in this size range are likely to exist on a rough copper surface. However, a nanostructured surface of the type considered here may have interstitial spaces that have mouth radii that are on the order of a few hundred nanometers. This indicates that a wall superheat on the order of 40°C or more would be required to achieve a critical radius size that would match the effective mouth radius of the very small cavities in the nanostructured surface and initiate nucleation.

These observations suggest that, compared to plain rough metal surfaces, the onset of nucleate boiling (ONB) for nanostructured surfaces with perfectly uniform interstitial spaces (and hence surface cavities) will require much larger superheat levels to initiate ONB. However, real stochastic surfaces, like those considered here, typically have variable cavity sizes, and ONB can be initiated by larger-than-average size cavities on the surfaces. Nevertheless, because of the generally smaller cavity sizes for nanostructured surfaces, ONB for such surfaces may occur at higher surface superheat levels than for rough plain metal sur-

faces, and the variation of the number of active nucleation sites per unit area with superheat may vary in a manner that is quite different from conventional metal surfaces with a nearly continuous distribution of cavity sizes. The focus of the study described here is to explore how the variation of the number density of active nucleation with superheat is affected by the surface morphology for nanostructured surfaces that have some larger surface irregularities that may become active nucleation sites. Understanding this connection is centrally important to developing strategies for enhanced boiling surface design that produce surfaces with the wicking advantages of a nanostructure coating and the low onset of boiling superheat that results from a limited number of larger-scale interstitial spaces in the surface coating.

2. DROPLET DEPOSITION ON A HEATED NANOSTRUCTURED COATED COPPER SUBSTRATE

In addition to the additional insight into pool boiling by performing droplet deposition experiments, this method was also selected because it has demonstrated to give good results [3, 8, 9]. Based on the work done by the previous researchers, copper was selected as the substrate material due to its favorable thermal properties. Fabrication of the copper substrate and growth of the ZnO nanostructured surface were performed as follows:

- 1. A cylindrical 25.4 mm diameter rod was machined to a length of 25.4 mm and holes were drilled 180° from each other near the surface of the end of the machined cylinder which would be late used for thermocouple placement. The bulk material portion of the substrate was finished off with a tapped hole at the opposite end of the cylinder to be used for the ZnO growth procedure.
- 2. The top surface of the substrate was sanded to a mirror-like finish to prepare it for the growth of the nanostructures.
- The substrate was then cleaned by ultrasound through successive ultrasonic baths of acetone, isopropyl alcohol, and distilled water to ensure the surface was void of contaminants before proceeding with the growth procedure.
- 4. Two solutions were then prepared for the growth procedure:
 - Distilled water, Hexamethylene Tetraamine, and Zinc Nitrate Hexahydrate to enable nanostructure growth
 - ZnO nanoparticles and ethanol for seeding on the copper substrate sonicated to ensure even distribution of the particles
- 5. The copper substrate was heated to 120°C then the top surface was submerged in the nanoparticle solution. This process was repeated until the surface had a uniform appearance. The substrate was then suspended above a beaker of the growth solution so the surface was submerged and heated in an oven for 8 hours at 90 °C.

The resulting substrate was a copper test piece with a ZnO nanoparticle surface to be used in evaporation experiments.

2.1 Experimental Procedure

The substrate was then used to perform evaporation experiments of water droplets deposited on the nanostructured surface.

The experiments allowed for characterization of the surface via contact angle and capture of high speed videos of the evaporation process at various superheat levels and droplet volumes to be analyzed for nucleation sites and time for complete droplet evaporation.

Two types of droplet deposition experiments were performed, adiabatic and heated, each type was captured using a high speed video camera set to 2100 fps. For the adiabatic case, a known volume of the liquid was deposited onto the insulted substrate, which would be used to measure the contact angle. For heated evaporation experiments the substrate, surrounded by insulation to mitigate heat loss from the sides of the substrate, was placed on a hot plate which was then set to a few degrees above the desired temperature to ensure the substrate reached the desired temperature. The temperature was monitored via two thermocouples inserted into the pre-drilled holes. A droplet of a known volume of distilled water was deposited at a negligible height from the surface and the droplet was vaporized. This process was performed for droplet volumes 5-8 μ L and superheat values beginning at 10 °C and increasing in increments of 5 to 40 °C.

2.1.1 Post-Processing. The resulting videos from the adiabatic surface characterization and evaporation experiments underwent two post processing procedures using Adobe Premier Pro and ImageJ.

The adiabatic videos were imported into Adobe Premier Pro and frame by frame analyzed to capture the frame just before the transition of the droplet from synchronous spreading to hemispreading. The droplet footprint area was then measured from this frame using ImageJ with physical measurements of the substrate diameter to establish a scale. From the measurement of the droplet footprint area, the droplet footprint radius was then calculated by idealizing it as a spherical cap. Where the initial droplet footprint radius, $R_{s,0}$, is a function of the apparent contact angle, θ_{app} , and the initial droplet volume, $V_{d,0}$:

$$R_{s,0} = \left(\frac{3V_{d,0}}{\pi(2 - 3\cos(\theta_{app}) + \cos^3(\theta_{app}))}\right)^{1/3} \sin(\theta_{app}) \quad (2)$$

With the measurement of the footprint radius and a known droplet volume, the apparent contact angle was then solved for. The contact angle was computed for each of the five adiabatic experiment replications using the relationship from Eq. 2. This process was repeated for each day experiments took place resulting in two contact angles of 4.409° and 4.883°.

Similar to the adiabatic experiments, each heated experiment video was imported into Adobe Premier Pro to allow for analysis of each video frame. The video was scrubbed through to find the moments corresponding with the droplet first making contact with the surface and when the droplet completely evaporated. The total evaporation time was then able to be calculated by taking the difference between the two reference frames.

2.2 Visual

In addition to the quantitative measurements that resulted from the droplet experiments, the collected videos allowed for a visual analysis as well. As the heated experiment videos were being analyzed for evaporation time, observations were taken

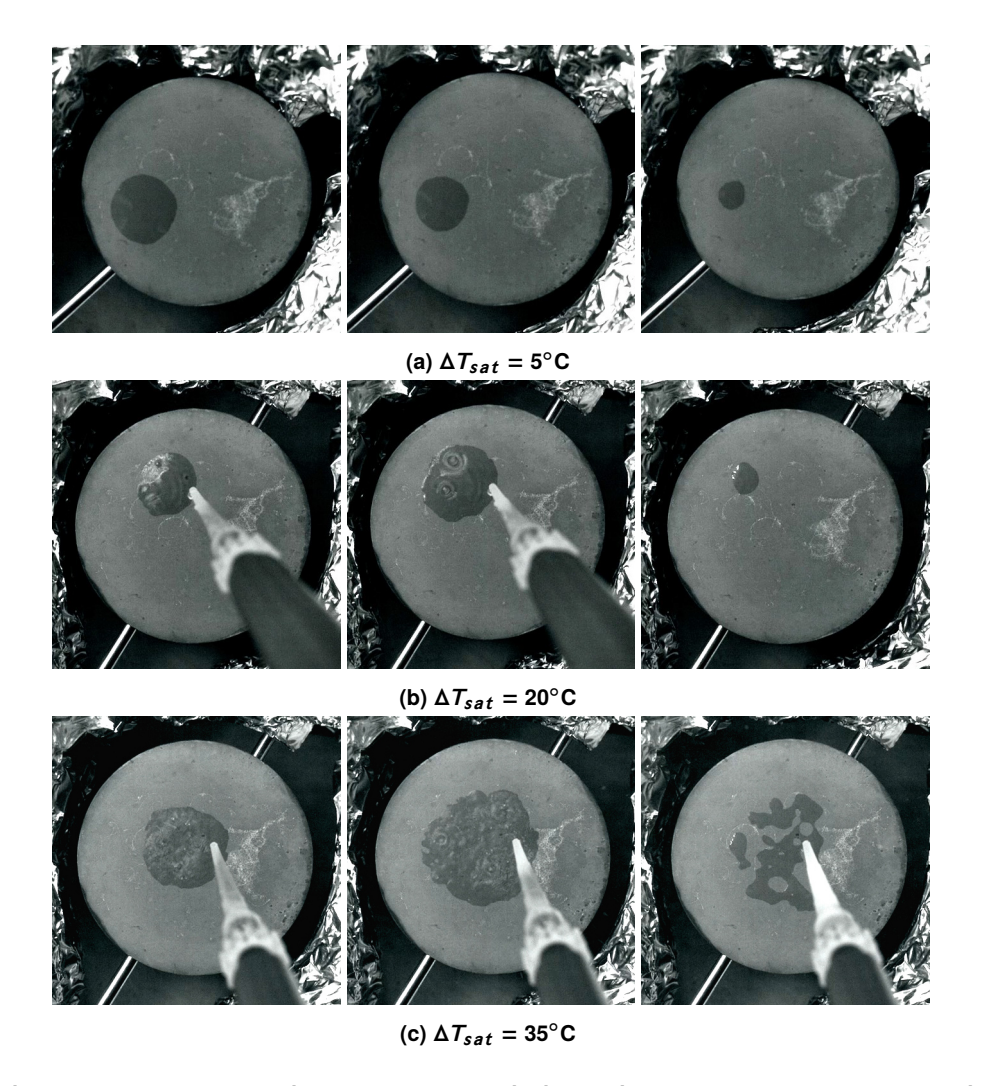


FIGURE 3: Sequential video frames of the evaporation of 8 μ L droplets with increasing superheat, where the leftmost images are immediately after droplet deposition, the middle images are midway through the evaporation, and the rightmost are just before total evaporation.

on when bubble nucleation occurred. For this nanostructured surface, superheat values below 10°C are postulated to be conduction dominated because this is below the temperature range where ONB occurs. The onset of nucleate boiling is believed to occur between 15°C and 20°C and beyond those values are considered well into the nucleate boiling dominated regime. Each of these regimes was physically observed during the heated experiments in this study and can be seen in Fig.s 3a, 3b, and 3c. These results indicate the onset of nucleate boiling for this surface occurs at around 15°C which is well below the superheat required for a nano-scale critical bubble radius, Fig. 2.

3. SEM IMAGING OF NANOPILLARS

As a step in the experimental process, images are taken of the ZnO surface using a scanning electron microscope (SEM). This process is generally used to gauge the success of the growth process previously described. Here it is also used to observe the cavity sizes present on the surface.

From Fig. 3b it can be seen that the onset of nucleate boiling was observed at superheat values below the required superheat for nano-scale critical radii indicating the likely presence of cavities

larger than the nano-scale. The surface was imaged with the intent to detect the suspected micron-scale cavities. Using a high speed video from the evaporation experiments and nucleation site characterization, the approximate location of a nucleation site was used as the origin for imaging. Images were taken from the approximate nucleation site and +/- 0.1 mm in x and y directions. Figures 4, 5, and 6 are a result of imaging the test surface fabricated for this study at various locations on the surface. The micrographs confirmed the existence of micron-scale cavities - in Fig. 5 cavities of approximately 1 and 2 μ m are observed and Fig. 6 captured a cavity at approximately over 3 μ m in length. Although larger scale cavities were observed, the majority of the surface was nano-scale stochastic pillars as seen in Fig. 4.

From the observed varying cavity sizes, we can postulate that the portion of the surface with a majority of stochastic nanopillars contributes to the hydrophyllic characteristics of the surface (ultra low contact angle) and conversely, the inclusion of micron-scale cavities enable the onset of nucleate boiling at temperatures between 15°C and 20°C. It then follows that the surface used in this study has superior performance capability because it combines

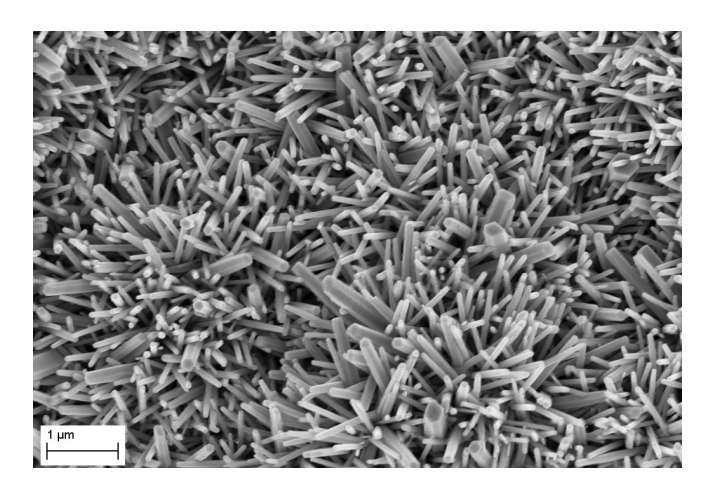


FIGURE 4: Micrograph of the surface demonstrating nanoscale ZnO nanopillar spacing without marked irregularities.

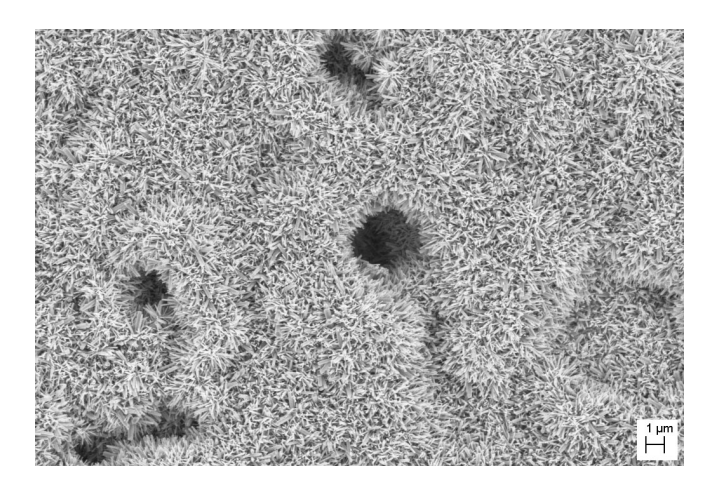


FIGURE 5: Observed micron scale cavities among nanoscale pillars on the surface.

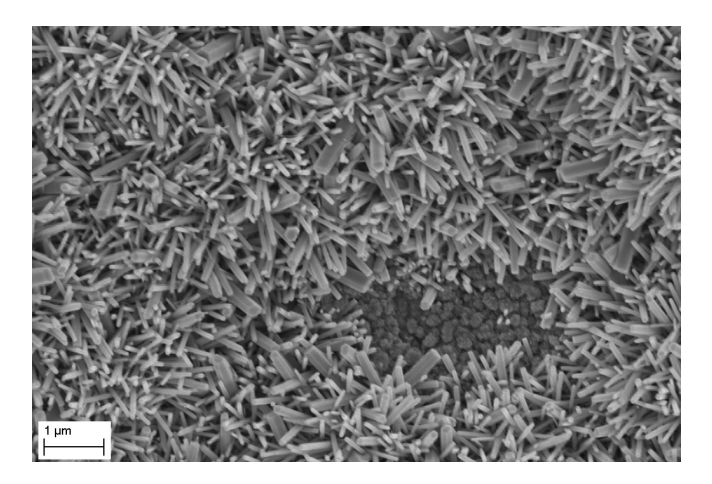


FIGURE 6: Cavity of the scale of roughly 3 μ L captured via SEM on the surface.

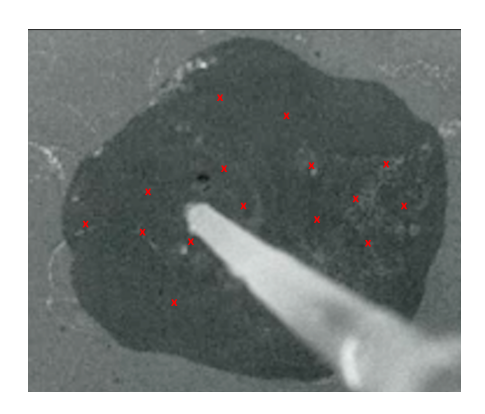


FIGURE 7: Example result of nucleation site counting procedure with markers representing observed sites.

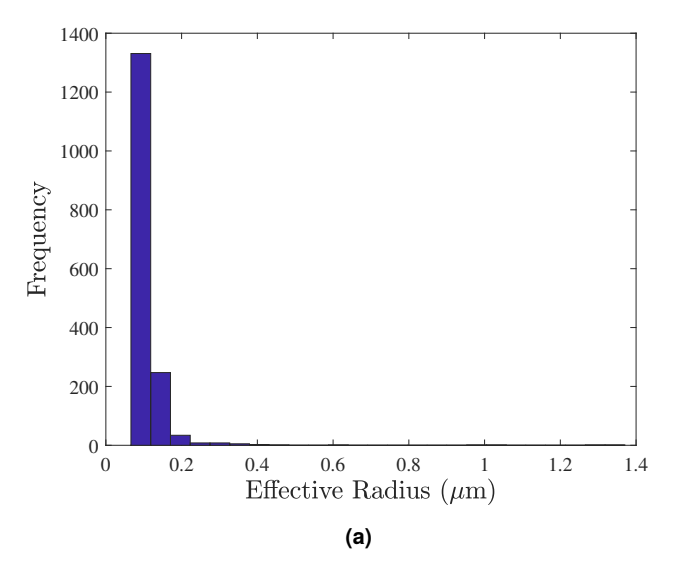
the desirable wicking characteristics of the nanostructures with the micro-scale features which can become active nucleation sites at modest temperatures. This leads to the desire to explore and verify this new mixed structure and corresponding high performance (ONB at low superheats), high rate of heat transfer, and maximum heat flux.

4. HIGH SPEED VIDEO ANALYSIS FOR NUCLEATION SITE CHARACTERIZATION

To fully characterize the substrate nanopillar coating, high speed videos from each experimental condition (all data points) were analyzed to determine the observed number of active nucleation sites over the evaporation process. The process began with opening the videos in Adobe Premier Pro where each frame of the video could be analyzed. The video was scrubbed to find the maximum droplet footprint area; the frame where the largest footprint area was observed was saved to be used as a reference for the remainder of the analysis. The frame was then imported to a simple presentation program which allowed for insertion and manipulation of diagrams to be used to mark the approximate location of the nucleation sites. Once the two software programs were set up, the high speed video was set to start at the instance of deposition. Each frame was stepped through, if a bubble was observed, a marker was inserted on the presentation software at the approximate corresponding location. If an there was an existing marker in the location of the observed nucleation site, no additional markers were added. As the video progressed, markers continued to be added until the final result was an image with markers corresponding the each observed nucleation site throughout the evaporation process, see example result in Fig. 7.

The analysis process began at superheat levels of $10~^{\circ}\text{C}$ and a droplet volume of $5~\mu\text{L}$ and spanned all experimental conditions used here. When analyzing videos of experiments at higher superheat levels, the droplets were well into the nucleate boiling regime making distinguishing individual nucleation sites extremely difficult. Nucleation site data at $40~^{\circ}\text{C}$ superheat was still collected but was excluded from nucleation site density analysis for this reason. In a similar fashion described in the contact angle measurement process, the captured images of the observed maximum droplet footprint were used in ImageJ to measure the footprint area. With the two pieces of information, the nucleation

site density, number of nucleation sites per unit area, was then calculated for all data points.



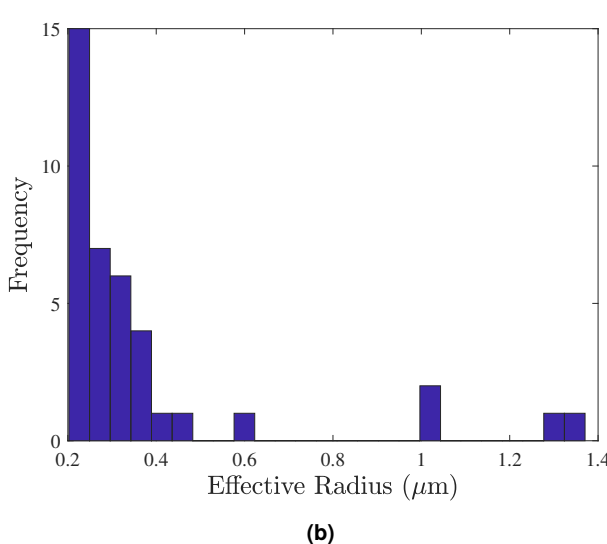


FIGURE 8: Distribution of representative pore sizes on the nanostructured surface and the distribution with the smallest pore size removed to display larger size counts.

5. PORE SIZE, POROSITY, AND ENTROPY

In addition to the macro-scale active nucleation site characterization, analysis was done to understand the cavity size distribution for a representative portion of the surface. A micrograph was selected, Fig. 5 from the previously described imaging which captured both nano-scale and micro-scale pores. This image was then processed using a Matlab script developed by Rabbani and Ezeakacha et al [10, 11]. The script is designed to take an input SEM image and the number of microns per pixel and count the visible number of cavities and measure their radius. The initial pore size distribution, Fig. 8a, produces an expected distribution with the majority of the pores having a radius of less than 100 nanometers. To better visualize the larger pore size cavities, a closer look was taken into cavities with pores larger than 200 nm in Fig. 8b where the visual larger cavities seen in Fig. 5 are

quantified. This evidence follows the logic of the existence of larger cavity sizes enabling nucleation at lower superheat levels than would be required for a nano-scale critical radius.

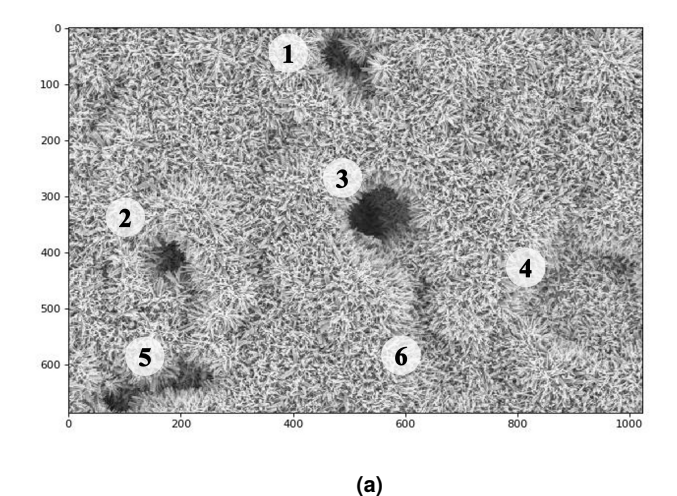
The number of micron-scale cavities does not in itself dictate the ability of a site to become an active nucleation site. It is postulated here that in addition to the presence of micron-scale cavities, the cavities must also be low in surface complexity (entropy) for the site to become an active nucleation site. The Python image processing package scikit-image contains a function which analyzes an input image by the amount of entropy contained in the image corresponding to the complexity of the image by detecting subtle variations in the local gray level distribution [12]. This package was used to generate images of surface entropy for the surface used in this study. The same representative SEM micrograph selected for the pore size distribution analysis, Fig. 5, was also selected to be analyzed with scikit-image because of the presence of cavities of various characteristics, those with low perceived surface entropy (area is void of nanostructures) and high perceived entropy (large scale cavity with nanostructures), see Fig. 9a. In Fig. 9a cavities have been labeled 1-6 corresponding to the visually detected micron-scale cavities. This image was then processed using the scikit-image package and the output was a corresponding entropy map which has also been labeled 1-6 to correspond with the input image cavity locations. Figure 9 demonstrates the complexity of each of the identified cavities - sites 1-3 are visually void of nanostructures in Fig. 9a and are characterized by relatively low corresponding entropy values in Fig. 9b. Conversely, if we observe cavity sites 4 and 6, by visual observation, the cavity sizes are relatively large, however, the corresponding entropy values are on the high end of the range, Fig. 9b. In the middle range is site 5 where a large cavity is observed with moderate entropy.

The experimental results from this study demonstrate the onset of nucleate boiling at moderate temperatures is due to the presence of these larger micron-scale cavities which are also largely void of nanostructures. It is then postulated that if the desired surface coating is to be composed of nanostructures and micron-scale cavitities to achieve desired wicking and moderate temperature ONB, then the ideal micron-scale cavities would have increased likelihood of becoming an active nucleation site if it has low surface entropy. This is due to the observations of micron-scale cavities with high entropy containing nanostructures which would then reduce the critical radius and increase the superheat required for nucleate boiling. Figure 10 depicts the region in which the larger micron-scale cavities with low surface entropy occur; this the region with an increased probability of the occurance of an active nucleation site at modest superheat levels.

6. NUCLEATION SITE DEPENDENCY ON SURFACE MORPHOLOGY

Various nucleate boiling models have been developed in which the bubble departure diameter has been selected as the length of scale and each argues that the nucleation site density is proportional to the superheat to some power, $m, n'_a \propto (T_w - T_{sat})^m$ [13–15]. Specifically, Tien [13] proposed a model that predicts heat flux

$$q'' = 61.3Pr_l^{0.33}k_l(T_w - T_{sat})(n_a')^{0.5}$$
(3)



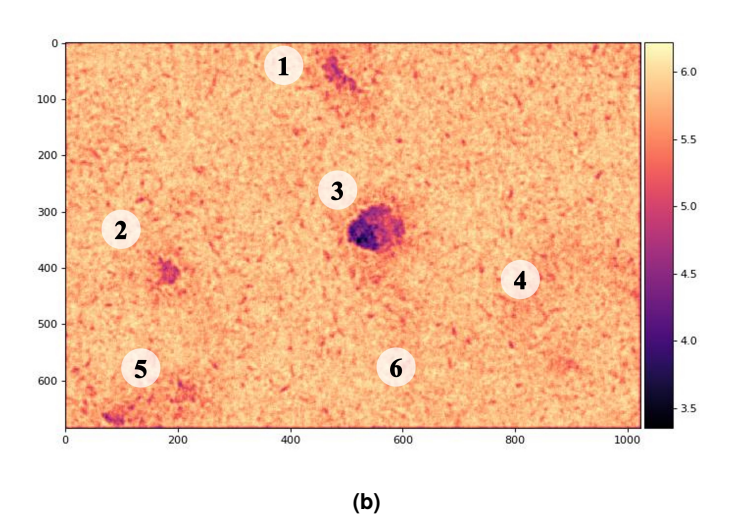


FIGURE 9: SEM image of the surface with cavities on the micronscale in (a) and the corresponding entropy analysis of the micrograph in (b). Large cavities visually present are numbered 1-6.

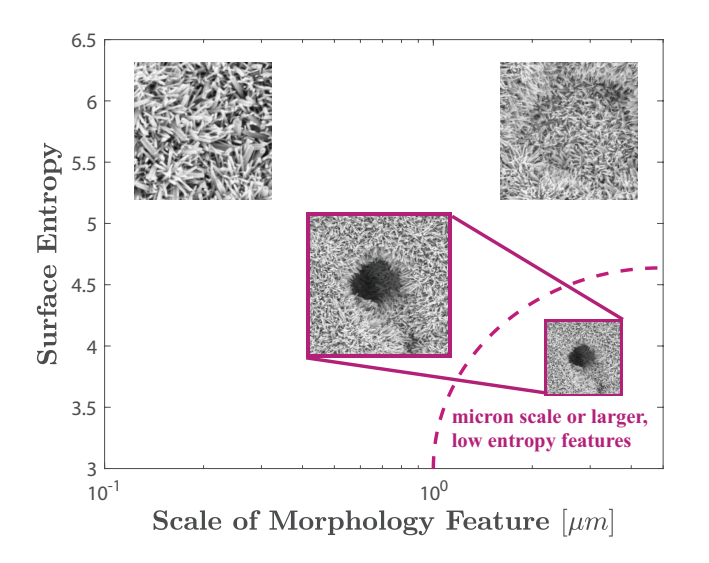


FIGURE 10: Representative boundary where micron-scale cavities with low surface entropy occur.

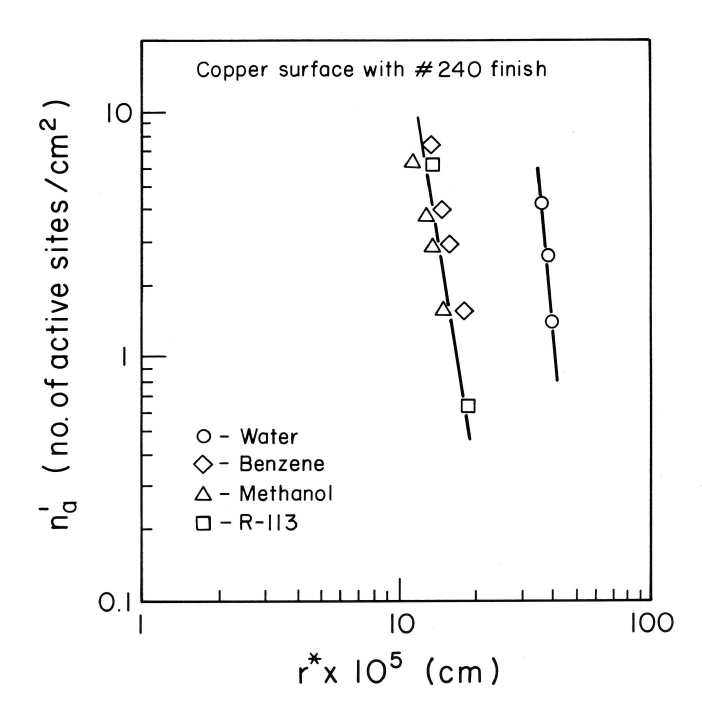


FIGURE 11: Critical radius versus observed nucleation site density for a plain copper substrate as observed by Lorenz [16].

and because $q'' \propto (T_w - T_{sat})^3$ for nucleate boiling, it follows that the nucleation site density must be proportional to superheat to the 4th power

$$n_a^{'} \propto (T_w - T_{sat})^4 \tag{4}$$

This line of reasoning is further supported when observing Fig. 11 where Lorenz et al. demonstrates the relationship of nucleation site density with critical radius for various liquids on a plain copper substrate [16]. It is understood that the critical radius is inversely proportional to superheat, therefore the observed that the slope for water corresponds with superheat to the 4.5 exponent for a plain surface. Our surface here is distinctly different because it contains two distinctive features of the nanostructured pillars and the larger cavities. This morphology presents almost a bimodal behavior for the ONB. To understand the interaction of nucleation site density and level of superheat for the surface here, the two were plotted for all data points generated in this study. Figure 12 depicts nucleation site can be approximately fit with a curve where it is proportional to superheat to the 1.28 power.

These observations from previous researched on a plain surface and our results therefore indicate a weaker increase in active nucleation sites with increasing superheat than generally observed for nucleate boiling of conventional metal heated surfaces. For conventional metal surfaces, the dependence of active site density on superheat is dictated by the combined effect of the distribution of cavity sizes on the surface, and the relation between the temperature dependence of the bubble equilibrium radius. This suggests that the distribution of interstitial space cavity sizes for our nanostructured coating is distinctive with a smaller number of larger cavities, widely spaced in size categories so that larger increases in temperature are required to increase the number of

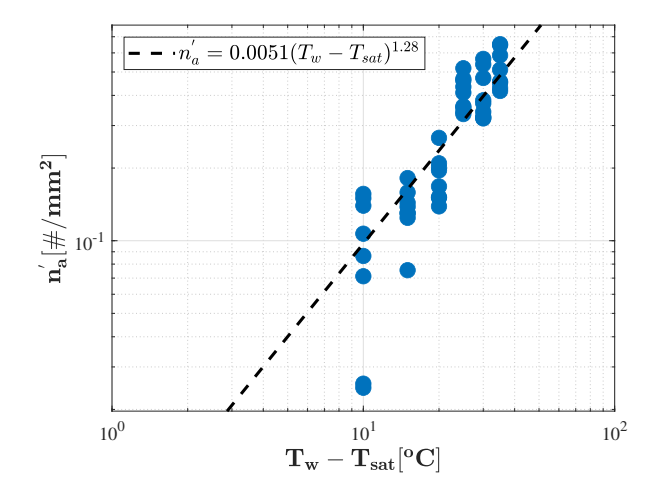


FIGURE 12: Observed nucleation site density and dependence on temperature for water droplets on the nanostructured surface tested here at atmospheric pressure. Included is a generated exponential fit to the experimental data.

activated nucleation sites. This can be explored more quantitatively as follows.

$$\frac{dn'_c}{dr_m} = F(r_m) \tag{5}$$

Where F is the distribution function for n_c , the number density for cavities (#/mm²) on the surface as a function of effective mouth radius r_m . Solving for the number density of active sites from Eq. 5 where the function $F(r_m)$ is postulated as

$$F(r_m) = br_m^{-\gamma} \tag{6}$$

The number density of active sites corresponds to those with effective mouth radius values greater than the critical radius r^* , where

$$r* = \frac{2\sigma T_{sat}(P_{sat})\nu_{lv}}{h_{lv}(T_{w} - T_{sat})}$$
(7)

Then the active site density is

$$n'_{a} = \int_{r_{*}}^{\infty} F(r_{m}) dr_{m}$$

$$= \left[-\frac{b}{1 - \gamma} r_{m}^{-\gamma} \right]_{r_{*}}^{\infty}$$

$$= -\frac{b}{1 - \gamma} r_{*}^{1 - \gamma}$$

$$n'_{a} \propto r_{*}^{1 - \gamma} \propto (T_{w} - T_{sat})^{\gamma - 1}$$
(9)

From our data of observed nucleation site density, the data has been fitted to a curve in Fig. 12 in which the indicated exponent is 1.28. It follows then that for our surface $\gamma - 1 = 1.28$ and $\gamma = 2.28$. Substituting in for the definition of the number density of cavities distribution function Eq. 5,

$$\frac{dn'_c}{dr_m} = F(r_m) \propto r_m^{-2.28} \tag{10}$$

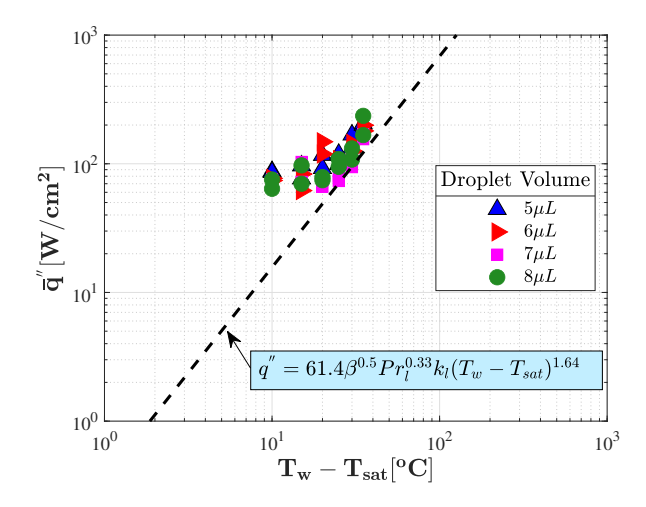


FIGURE 13: Mean heat flux calculated per unit area variation with superheat for water droplets on the nanostructured surface tested here at atmospheric pressure and heat flux curve fit developed following Tien's model.

This also implies that

$$n_a' = \beta (T_w - T_{sat})^{1.28} \tag{11}$$

where β = 5100. This allows for the adaptation of Tien's model for a plain surface to one with a nanostructured surface which takes the form

$$q'' = 61.3\beta^{0.5} Pr_I^{0.33} k_I (T_w - T_{sat})^{1.64}$$
 (12)

Independently, the heat flux was calculated for the experimental data points. This was plotted in Fig. 13 along with the adapted heat flux model Eq. 12, where the experimental heat flux values follow the model fairly well.

7. INTENTIONAL INTRODUCTION OF MICRON-SCALE CAVITY SITES

Observations from experiments with the nominally smooth coated substrate described thus far indicate that sites of micronscale cavities formed during nanostructure synthesis are the location of bubble nucleation during the droplet evaporation process. These desirable features of the coating are likely due to small scale defects on the surface of the copper. We hypothesized that deliberate creation of micron-scale cavities on the substrate prior to nanostructure growth would carry through the synthesis process and increase the number of observable active nucleation sites via the combination of cavities with a defect origin and those intentionally added. A second substrate was fabricated with physically introduced score marks of approximately 40 µm width in a grid pattern of 9x9 with 1 mm spacing, centered on the surface of the substrate. The score marks were created using light pressure applied to a needle positioned with 3D printed fixtures to control the spacing of the lines during the scoring process. The scored substrate was then prepared, coated, and experimentally tested following the same procedure as the nominally smooth substrate described in Section 2. Similarly, results from the experiments were then processed as described in Sections 4 and 5.

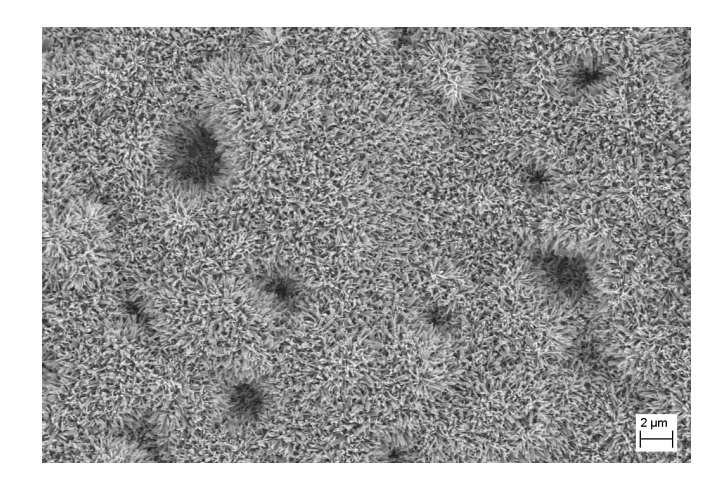


FIGURE 14: Representative micrograph of the scored substrate surface post synthesis of the nanostructures.

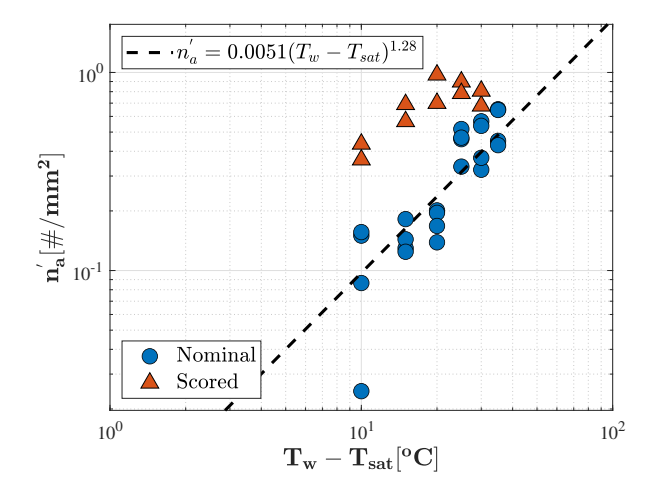


FIGURE 15: Observed nucleation site density and dependence on temperature for water droplets on the nominal nanostructured surface and the scored nanostructured surface tested at atmospheric pressure for droplet volumes of 6 and 8 μL . Included is a generated exponential fit to the experimental data.

The resulting micrographs indicated a successful synthesis process that produced an increased number of relatively large scale cavities amidst the nominal nanopillars, as shown in Fig. 14. When compared to the nominally smooth substrate micrograph, Fig. 5, the scored substrate, Fig. 14, has an apparent increase in number of larger scale interstitial cavities which are likely to lead to an increase of observed active nucleation sites. This was further confirmed through measurement of observed nucleation site density across superheats for droplet volumes of 6 and 8 μL . The density was significantly larger for the scored substrate when compared to that of the nominally smooth substrate. This is demonstrated in Fig. 15. Note the reduced differential of the nucleation site density at higher superheat levels. This is attributed to increased boiling causing difficulty in distinguishing individual active nucleation sites.

The surface of both the nominally smooth substrate and the scored substrate can each be represented by a multivariate dis-

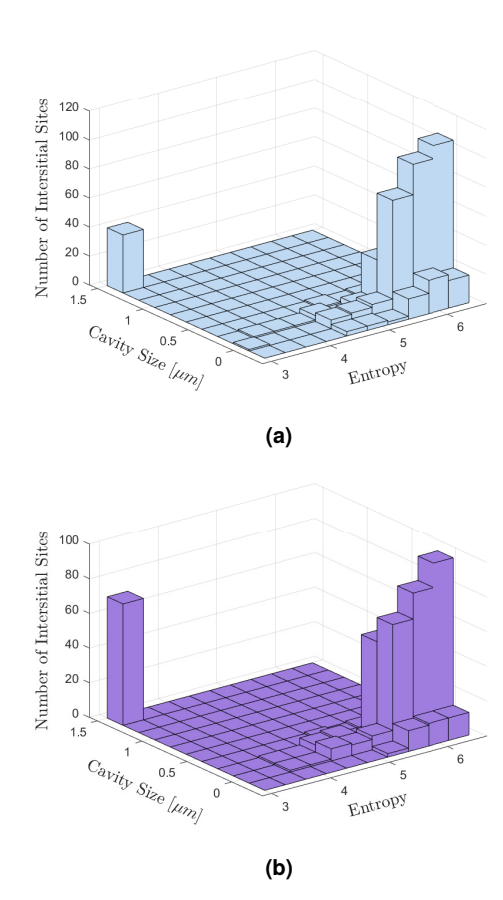


FIGURE 16: Illustrative distribution of interstitial cavities in nanostructured coating grown on a nominally smooth substrate (a) and an illustrative distribution of interstitial cavities in nanostructured coating grown on a scored substrate (b).

tribution of interstitial sites of varying scales and entropy levels. The results of our study indicate that an optimal morphology for an enhancing nanostructured coating is one with the bulk of the interstitial sites on the nano-scale with high entropy and a non-negligible number of micron-scale cavities with low entropy. Figure 16 depicts representative distributions for each of the substrate types where the z-axis is considered the number of cavity sites within the footprint of a droplet during evaporation; this correlates with the observed increase in active nucleation sites over the evaporation process.

8. CONCLUSION

This exploration of the morphology of ZnO nanostructures on a copper substrate and the impact on the onset of nucleate boiling demonstrated the phenomena observed by prior research [1, 5, 6] in which the experimentally observed superheat required for onset of nucleate boiling is well below the theoretically required superheat is related to the inclusion of micron-scale cavities. More specifically:

 Results of this study document that the thermally grown nanostructured coating we create on metal surfaces has a distinctive distribution of interstitial space size. The surface is mostly covered by a nanoporous coating, with a limited

- number of irregularities that are essentially interstitial space cavities that are micron-scale size. Our images analysis indicates these are larger micron-scale structures with low surface entropy.
- 2. Our analysis of observed nucleation site density as a function of surface superheat, using the Tien [13] nucleate boiling model, indicates that the distinctive bimodal surface structure results in a variation of active site with superheat that is much different that conventional rough metal surfaces. For our nanostructured surface, our results indicate that number density of active nucleation sites increase proportional to (T_{surf} T_{sat})^{1.28}, whereas Tien's [13] model analysis for conventional metal surfaces indicates that number density of active nucleation sites increase proportional to (T_{surf} T_{sat})⁴.
- 3. This understanding of the effect of surface morphology on this boiling mechanism obtained in this study is useful to efforts to design enhanced boiling surfaces. Also, our results indicate that limited larger micron-scale structures on an otherwise nanostructured surfaces can serve to be active nucleation sites at low to moderate superheat levels if their surface entropy is low (i.e., they have a simple void interstitial space structure). Results of this study also demonstrate that the deliberate inclusion of micron-scale substrate cavities prior to nanoporous layer growth results in an increase in observed active nucleation site density, which has potential to enhance the onset of nucleation capability and nucleate boiling heat transfer performance of enhanced boiling surface designs.

ACKNOWLEDGMENTS

Support for this research under National Science Foundation CBET grant number 2228373 is gratefully acknowledged. Partial funding for this research was also provided by the endowment of the A. Richard Newton Chair in Engineering at UC Berkeley.

REFERENCES

- [1] Carey, Van P., Wemp, Claire K., McClure, Emma R. and Cabrera, Samuel. "Mechanism Interaction During Droplet Evaporation on Nanostructured Hydrophilic Surfaces." Vol. Volume 8A: Heat Transfer and Thermal Engineering: p. V08AT10A029. Pittsburgh, PA., 2018.
- [2] Cabrera, Samuel. "Fabrication and Testing of Zinc Oxide Superhydrophilic Nanostructured Surfaces on Metal Substrates and Wavy Fin Geometries for Use in Spray Cooling." Ph.D. Thesis, University of California, Berkeley. 2022.
- [3] McClure, Emma. "Zinc Oxide Nanoporous Superhydrophilic Surfaces: A Synthesis of Experimental Durability Testing and Droplet Vaporization Model Development Using Machine Learning Methods." Ph.D. Thesis, University of California, Berkeley. 2021.
- [4] Padilla, Jorge. "Experimental Study of Water Droplet Vaporization on Nanostructured Surfaces." Ph.D. Thesis, University of California, Berkeley. 2014.

- [5] Wemp, Claire K. "An Exploration of Nanostructured Surfaces for Wicking and Vaporization Enhancement." Ph.D. Thesis, University of California, Berkeley. 2018.
- [6] Silva, Anisa D. and Carey, Van P. "Use of a Genetic Algorithm to Model the Interaction of Conduction and Nucleate Boiling Mechanisms During Evaporation of Water Droplets on Superheated ZnO Nanostructured Surfaces." Vol. ASME 2023 Heat Transfer Summer Conference: p. V001T02A005. 2023.
- [7] Carey, Van P. *Liquid-vapor phase-change phenomena*. Taylor and Francis (2020): Chap. 6.
- [8] Cabrera, Samuel and Carey, Van P. "Comparison of Droplet Evaporation and Nucleate Boiling Mechanisms on Nanoporous Superhydrophilic Surfaces." ASME 2019 Heat Transfer Summer Conference. 2019. ASME, American Society of Mechanical Engineers, NEW YORK.
- [9] Padilla, Jorge and Carey, Van P. "Water Droplet Vaporization on Superhydrophilic Nanostructured Surfaces at High and Low Superheat." Vol. Volume 8B: Heat Transfer and Thermal Engineering. 2014.
- [10] Rabbani, Arash and Salehi, Saeed. "Dynamic modeling of the formation damage and mud cake deposition using filtration theories coupled with SEM image processing." *Journal of Natural Gas Science and Engineering* Vol. 42 (2017). DOI 10.1016/j.jngse.2017.02.047.
- [11] Ezeakacha, Chinedum, Rabbani, Arash, Salehi, Saeed and Ghalambor, Ali. "Integrated Image Processing and Computational Techniques to Characterize Formation Damage." 2018. DOI 10.2118/189509-MS.
- [12] van der Walt, Stéfan, Schönberger, Johannes L., Nunez-Iglesias, Juan, Boulogne, François, Warner, Joshua D., Yager, Neil, Gouillart, Emmanuelle, Yu, Tony and the scikit-image contributors. "scikit-image: image processing in Python." *PeerJ* Vol. 2 (2014): p. e453.
- [13] Tien, C.L. "A hydrodynamic model for nucleate pool boiling." *International Journal of Heat and Mass Transfer* Vol. 5 No. 6 (1962): pp. 533–540.
- [14] Mikic, B B and Rohsenow, W M. "A new correlation of pool boiling data including the effect of heating surface characteristics (Nucleate pool boiling heat transfer data extended to relate effect of heating surface characteristics)." (1968): pp. 9P–9P.
- [15] Zuber, Novak. "Nucleate boiling. The region of isolated bubbles and the similarity with natural convection." *Intern. J. Heat Mass Transfer* Vol. 6 No. 1 (1963): pp. 53,IN1,61–60,IN2,78.
- [16] Lorenz, J. J., Mikic, B. B. and Rohsenow, Warren M. "The Effect of Surface Conditiona on Boiling Characteristics." *Proceeding of International Heat Transfer Conference 5*. 1974. Begellhouse.